Thin-Walled Structures 188 (2023) 110787

Contents lists available at ScienceDirect

Thin-Walled Structures

journal homepage: www.elsevier.com/locate/tws

Full length article

On the beam-to-beam eccentric end plate connections: A numerical study

Samet Eltaş [a,b], Mehmet Ali Güler [c], Konstantinos Daniel Tsavdaridis [d,*], Christos E. Sofias [e], Bora Yıldırım [a]

[a] Department of Mechanical Engineering, Hacettepe University, Ankara 06800, Turkey
[b] Microelectronics, Guidance and Electro-Optics Business Sector, ASELSAN Inc., Ankara 06011, Turkey
[c] College of Engineering and Technology, American University of the Middle East, Kuwait
[d] Department of Engineering, School of Science & Technology, City, University of London, EC1V 0HB, London, UK
[e] Democritus University of Thrace, Xanthi, 67100, Greece

ARTICLE INFO

Keywords:
Beam-to-beam connections
Eccentric end plate (EEP) connections
Parametric study using FE model
Semi-rigid steel joints

ABSTRACT

Beam-to-beam connections are widely used in steel structures, especially in large floor applications and in cases where they are dictated by architectural restrictions. This type of connection is often designed without rotational restrictions (pinned connections), leading to relatively high bending capacity demands for the connected secondary beam, particularly when larger spans are employed. A commonly used practice to limit the above mentioned effect is to design beam-to-beam fixed connections at both ends of the secondary beam. Although joints transferring bending moments are covered in EN-1993 Part 1–8, there is no standardization for beam-to-beam fixed connections, often resulting in questions about their rotational capacity. Moreover, there is very little guidance on the design of beam-to-beam connections in the open literature. Therefore, this paper presents a comprehensive investigation of the beam-to-beam eccentric end plate connections using finite element analysis following the experimental tests. The parametric study is conducted using experimental data to propose a reliable analytical model of structural behavior under monotonic gravitational loading. The eccentric end plate connection exhibited satisfactory rotational stiffness and bending capacity. The failure mechanism on the connection parts is also presented for a better evaluation of the key parameters affecting the connection's structural performance.

1. Introduction

Primary beams are generally used to bridge the span between the frame columns. In contrast, the secondary beams are connected to the primary beams and are used to ease floor load distribution and stiffen the slabs.

In a frame structure, these beams are connected using welded or bolted connections. These connections are either in the form of a single-sided type or a double-sided type configuration [1], completing the build-up of the frame structure.

Generally, connections are modeled to be either pinned or rigid. A pinned connection assumes that no moment is transmitted between the connected members. On the other hand, a rigid connection assumes that no relative rotation occurs between the connected parts. These simplified models are easy to use, but they usually do not accurately reflect the mechanics of the structure [2–5]. Research studies have shown that most connections operate between those nominal extremes and are known as semi-rigid connections [6–11]. It is well known that these connections can lead to energy dissipation under dynamic loads and increase the ductility capacity of the joints [12,13].

Many different types of joints can be used for beam-to-beam connections, such as fin plate (FP), partial-depth end plate (PDEP), eccentric end plate (EEP), T-stub, joints with additional plates, and top-seat angle joints [14–18]. Note that end-plate connections have received significant interest among these various forms of joints used in the structural steel industry owing to their low cost, ease of fabrication, and ease of installation, especially if complex geometries are needed.

Although many studies on beam-to-column steel connections exist in the literature, the studies on beam-to-beam connections are limited. Herein the most relevant research is presented. Lopez et al. [19] investigated beam-to-beam connections with an additional plate as one of the few studies published on this type of connection. They examined a component called "additional plate in bending", which is not covered by standards, and obtained an analytical characterization of the joint by performing experimental and numerical studies. It is concluded that the proposed additional plate in bending is the most relevant

* Corresponding author.
E-mail addresses: samet_eltas@hotmail.com (S. Eltaş), mehmet.guler@aum.edu.kw (M.A. Güler), konstantinos.tsavdaridis@city.ac.uk (K.D. Tsavdaridis), chsofias@gmail.com (C.E. Sofias), boray@hacettepe.edu.tr (B. Yıldırım).

https://doi.org/10.1016/j.tws.2023.110787
Received 30 October 2022; Received in revised form 10 April 2023; Accepted 14 April 2023
Available online xxxx

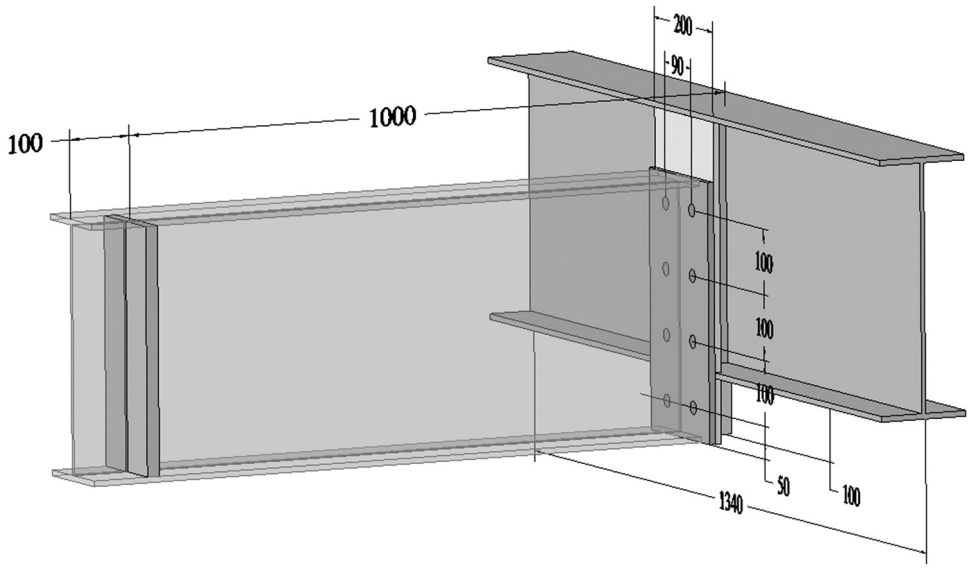

Fig. 1. Dimensions of the EEP connection base model.

Table 1
Material properties.

Components	Material Properties			
	f_y [MPa]	f_u [MPa]	Young's Modulus [GPa]	Tangent Modulus [MPa]
Grade S355 Steel	391	528	180	5000
M20, Grade 8.8 Bolt	640	800	180	750

component contributing to the stiffness and resistance of the structure. Urbanos et al. [20] studied the effects of bending, tension, and compression on semi-rigid beam-to-beam end-plate bolted joints with the component method and numerical analysis. They recommended that if significant axial forces were acting on the joint, the design should include the combined effects of the bending and the axial force. Natesan et al. [21] investigated the failure behavior of two different beam-to-beam arrangements. The first type was the clip angle connection between the two beams, and the second type was the flange strip connection between the two beams. Local buckling, distortion buckling, and small bearing deformation of the bolt hole were observed in the former, whereas pullout failure was observed in the latter. Mohamadi-Shooreh et al. [22] proposed a predictive empirical model based on beam section, end plate configuration, and bolt property to depict the moment–rotation relationship of bolted flush end plate beam-to-beam connections. They proposed an equation involving a three-parameter exponential function that can produce acceptable results regarding moment–rotation behavior. Hawxwell and Tsavdaridis [23] studied three different beam-to-beam connection types (FP, PDEP, and EEP) experimentally and found that the EEP connection had stiffer behavior than the FP and PDEP and was categorized as semi-rigid.

This paper presents a numerical model and a comprehensive parametric study on the EEP beam-to-beam connections as a follow-up investigation of the experimental work of Hawxwell and Tsavdaridis [23]. A finite element (FE) model is developed and validated using the experimental results provided in [23]. Therefore, this study presents a detailed investigation of the effects of several parameters, including the thickness of stiffeners and end plates, secondary beam span length, secondary beam section size, and differences in the level of beams on beam-to-beam EEP connection characteristics. In addition, the effect of two different primary end plate types, namely, Full Depth Primary End Plate (FDPEP) and Partial Depth Primary End Plate (PDPEP) are investigated on joint behavior. Lastly, the effect of removing some bolt rows on the moment–rotation characteristics of the connection is studied.

2. FE model of the EEP connection

This section explains the FE model of the original baseline design in detail. Static analysis is performed to simulate the monotonic loading application in the experimental study. Fig. 2 illustrates both its direction and position on the secondary beam.

2.1. Model geometry

The geometry consists of two main parts, namely, a primary beam and a secondary beam which are joined through connecting members. The three-dimensional solid model of the EEP connection is illustrated in Fig. 1. The experimental setup and the CAD model also are shown in Fig. 2. The details of the connection members are shown in Fig. 3. For the base model, the thicknesses of the upper and the lower stiffeners are $t_1 = 10$ mm, and the thicknesses of the end plates are $t_2 = 10$ mm. The primary and secondary beams' section sizes are both $406 \times 140 \times 39$UB and are made of grade S355 steel, which is a typical UB section and steel grade used in both British and European construction practices. Primary and secondary beams are not flush with each other; there is a 100 mm level difference (secondary beam is translated 100 mm from the primary beam in $-z$ direction) between them. Bolts are M20, grade 8.8.

2.2. Material properties

All components except bolts are S355 steel. A bi-linear isotropic hardening material model has been defined for each S355 steel and grade 8.8 bolt. Material properties for both S355 steel and M20, grade 8.8 bolt are obtained from the experimental study of [23] and are listed in Table 1. Poisson's ratio is 0.3 for all components.

2.3. FE bolt modeling

"BEAM188" ANSYS element type is used to model the circular bolt geometry, providing the option not to use any solid element

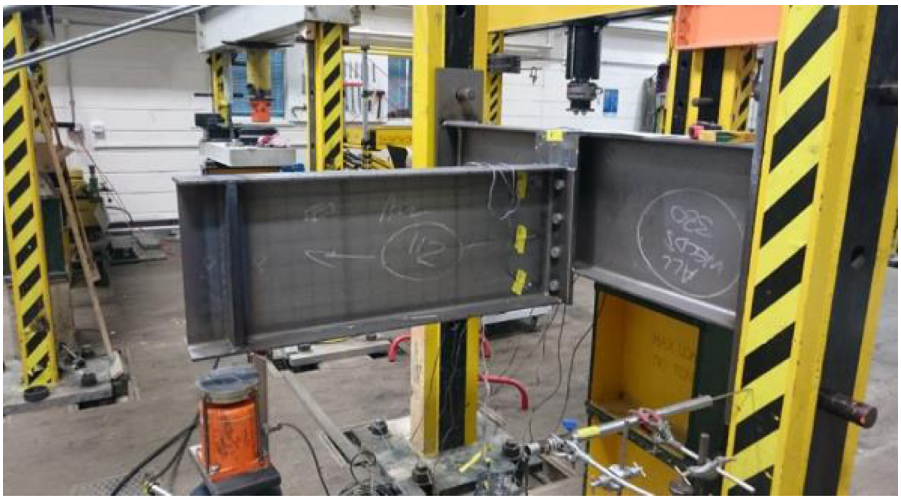

(a)

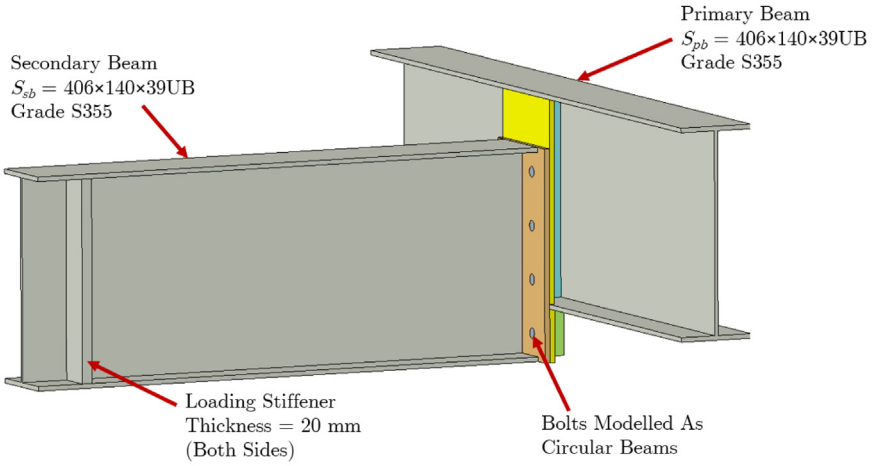

(b)

Fig. 2. The base model of the EEP connection (a) experimental setup [23] (b) 3D CAD geometry.

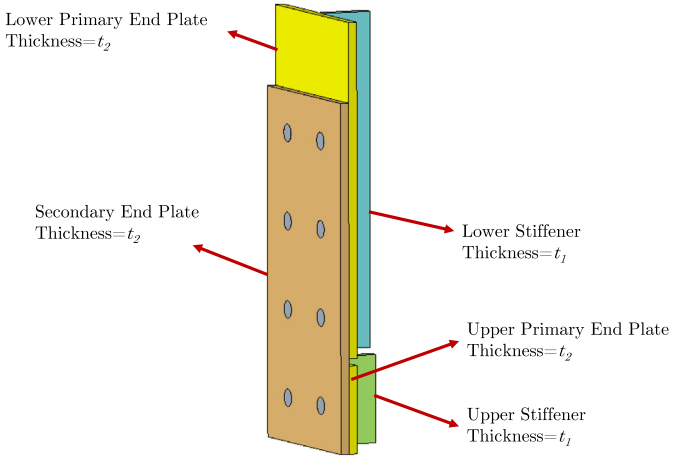

Fig. 3. 3D CAD illustrations of the EEP connection components.

description. The circular beam is a line element with a pilot node at each end. These nodes (I and J) are connected to imprinted areas that represent bolt and nut heads using multi-point constraints (MPCs), as shown in Fig. 4.

2.4. Boundary conditions

In the test configuration, the primary beam is connected to the test column using end plates at each end of the primary beam. The ends of the primary beam are considered to be rigid and hence constrained in all directions, as shown in Fig. 5. The load is applied in sub-steps with the option of auto-time stepping in ANSYS over the load stiffeners, 1 m away from the primary beam center-line as shown in Fig. 5. Loading is applied as a linearly increasing force from 0 up to at a value of which a component of the connection detail reaches the Ultimate Tensile Strength (UTS) of S355 steel. That means each ultimate moment value represents the strength capacity of the relevant connection detail. The analysis is presumed to be finished as soon as the UTS is detected in the stress value. The loading area is equivalent to the width of the beam (141.8 mm) multiplied by the thickness of the stiffener (20 mm) which equals 2,836 mm^2.

2.5. Beam rotation calculation

In the experiments conducted by [23], the deformations are measured using three LVDT gauges. Two LVDT gauges are located on

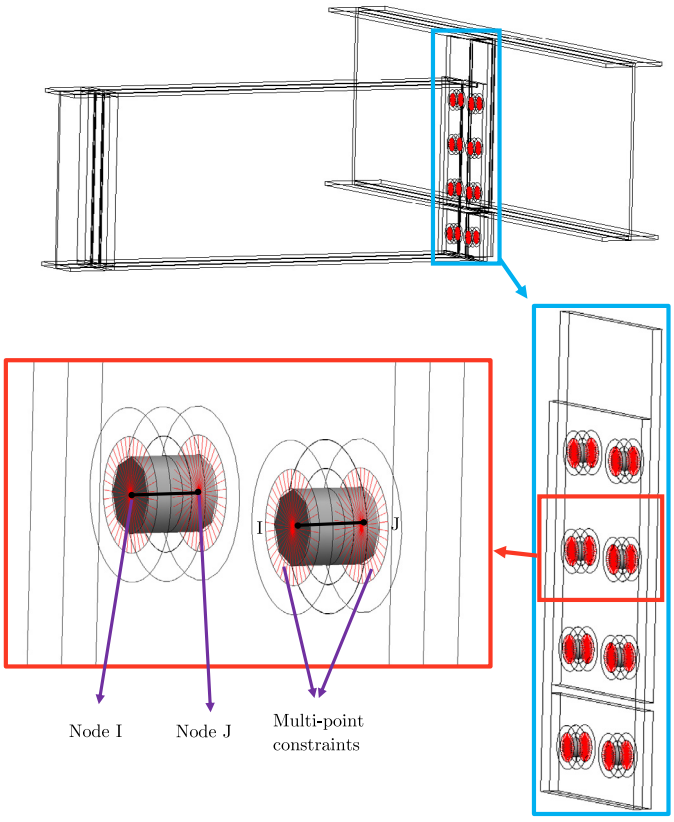

Fig. 4. FE bolt modeling.

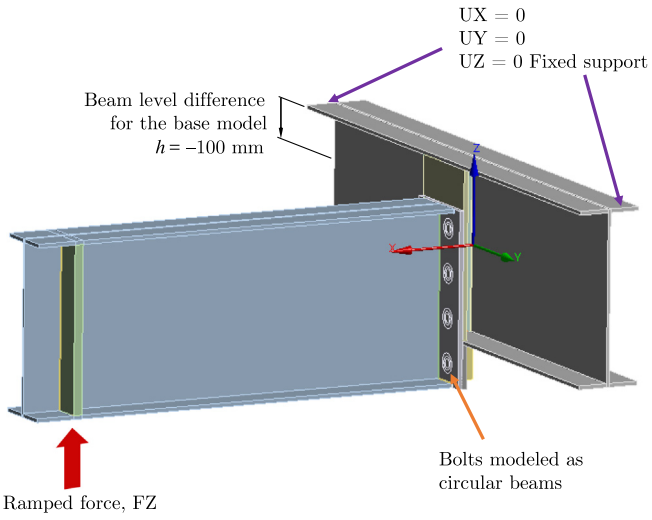

Fig. 5. Boundary conditions and applied load.

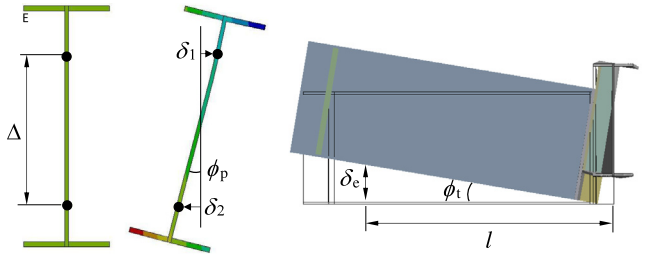

Fig. 6. Beam rotation calculation.

the back of the primary beam web at the beam centreline, 300 mm from each other, to measure the rotation of the primary beam. The deformations corresponding to these LVDTs are indicated as δ_1 and δ_2 in Fig. 6. The third LVDT is located at l = 850 mm away from the centerline of the primary beam web to measure end deflection δ_e. The trigonometry of the deformed beams under bending is used to calculate the rotation of the primary beam, ϕ_p, and the rotation of the secondary beam, ϕ_s, as follows.

$$\phi_p = \frac{\delta_2 - \delta_1}{\Delta}, \tag{1}$$

$$\phi_s = \phi_t - \phi_p, \tag{2}$$

where

$$\phi_t = \frac{\delta_e}{l}, \tag{3}$$

is the total rotation of the joint, and Δ = 300 mm.

2.6. FE mesh

The FE mesh used for the connection model is shown in Fig. 7. All the parts are modeled using the SOLID186 element type in the ANSYS library. A comparative study is done in order to determine whether to use linear or quadratic elements. It is concluded that the quadratic elements yield more accurate results than the linear elements. Fig. 8 shows the comparison in the load vs. end deflection and moment vs. rotation results for the element types (i.e., linear or quadratic).

2.7. Contact definitions

Two types of contact surfaces are defined in the FE model. The first one is the contact between two independent components in friction, and the second one is the welded surfaces. A sensitivity study is done by varying the friction coefficient, η, between 0.1 to 0.4 to determine its effect on the load vs. end deflection and moment vs. rotation results. It is concluded that whatever friction coefficient we choose (within this realistic range) does not have a major effect on the results, so we choose an expected middle-of-the-range value of η = 0.2. (see Fig. 9). On the other hand, welded components are defined in such a way that the components' surfaces' contact with the weld geometry is to be in bonded contact; however, frictional contact is defined between the directly interacting steel surfaces. In the contact regions, TARGE170 and CONTA174 element types are used to represent the contacts in the model.

2.8. Mesh convergence study

A mesh convergence study is conducted to determine the ideal element sizes in two different regions. Connection members and other parts are divided into two distinct size parameters, represented by a and b, respectively, as shown in Fig. 10. Finer mesh size is used in the vicinity of joint regions where high stress and strain gradients are expected to occur as in Ref. [24]. Mesh size parameters used in the mesh convergence study are given in Table 2. The results of the mesh convergence study are shown in Fig. 11. Furthermore, a single point for each plot has been taken as a benchmark result to calculate the percentage of error, and the results are presented in Tables 3 and 4. Moment vs. rotation results (see Table 3) show that the medium mesh type can be preferable regarding both result accuracy and time efficiency. However, when taking load vs. end deflection results (see Table 4) into account, it can be seen that the 'fine' mesh or the 'very fine' mesh stands out. The 'fine' mesh is selected to reduce the

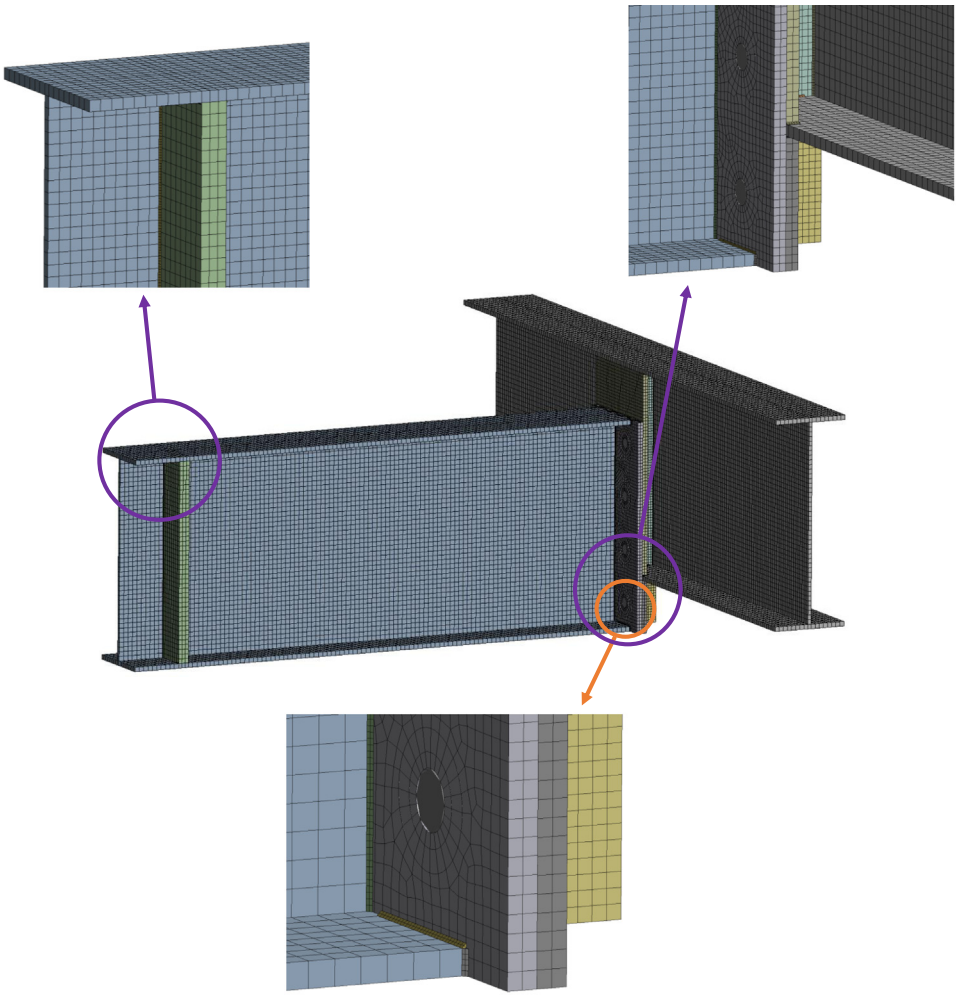

Fig. 7. FE mesh view of the base model.

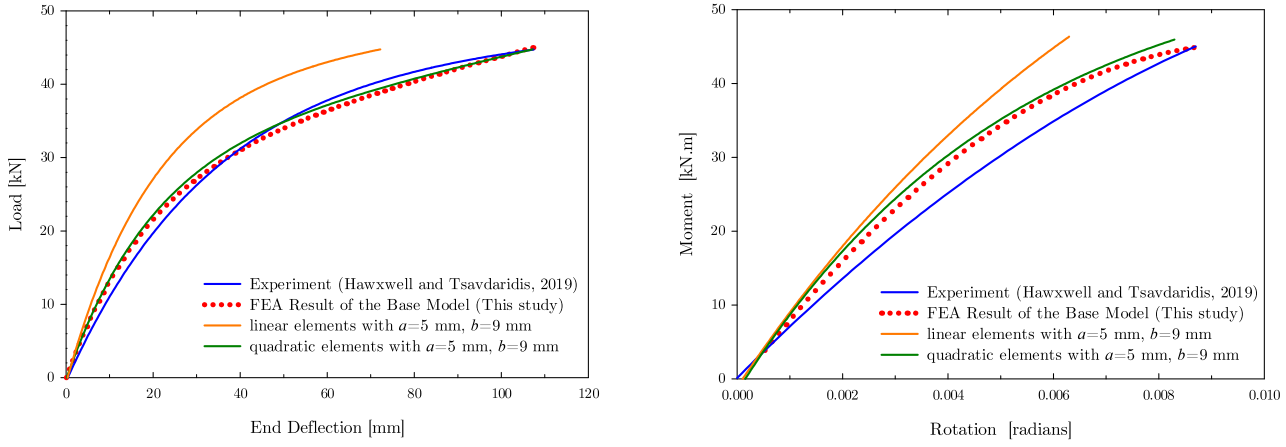

Fig. 8. The comparison of the element types used for meshing.

computational time. Using the 'fine' mesh size, elements and nodes reach approximately 41,000 and 265,000, respectively.

3. Results & discussion

In this section, the validation of the FE model is presented first. With the validated model, a comprehensive parametric study is conducted.

3.1. Validation of the FEA results against the experimental study

Force vs. end deflection and moment vs. secondary beam rotation graphs are used to compare experimental results and FE results for the base model. Load vs. end deflection and moment vs. rotation graphs are shown in Figs. 12 and 13, respectively. Good convergence is observed between the experimental and FE results, providing an accurate and

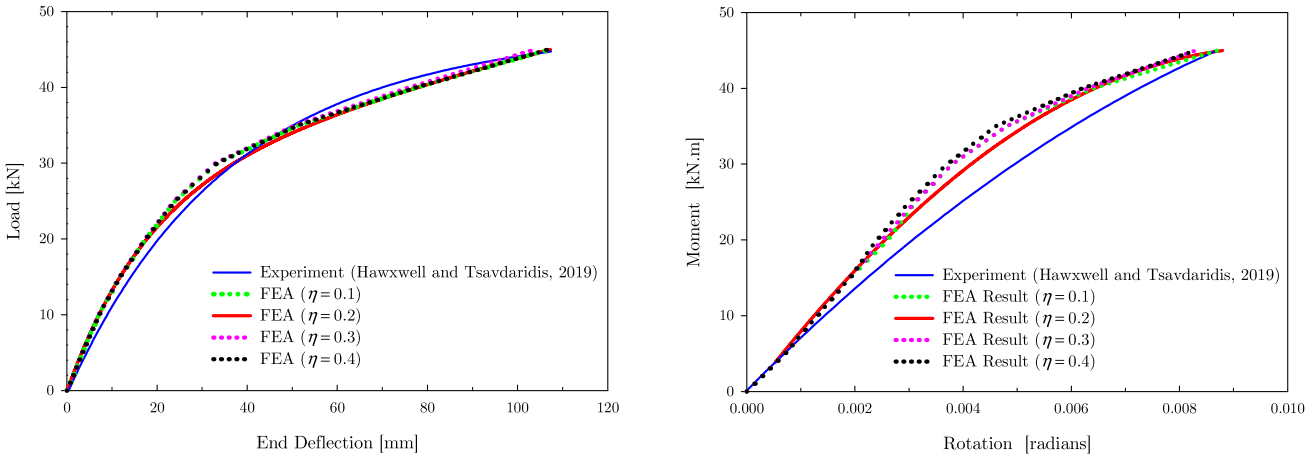

Fig. 9. Effect of varying the friction coefficient, η, used in the FEA model on the comparison with experimental results of Ref [23].

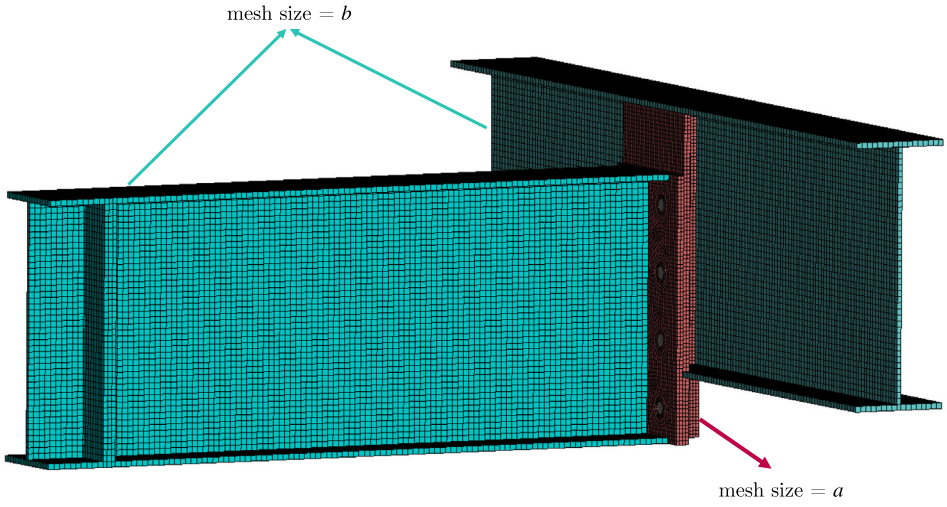

Fig. 10. Different mesh sizes used in the mesh convergence study.

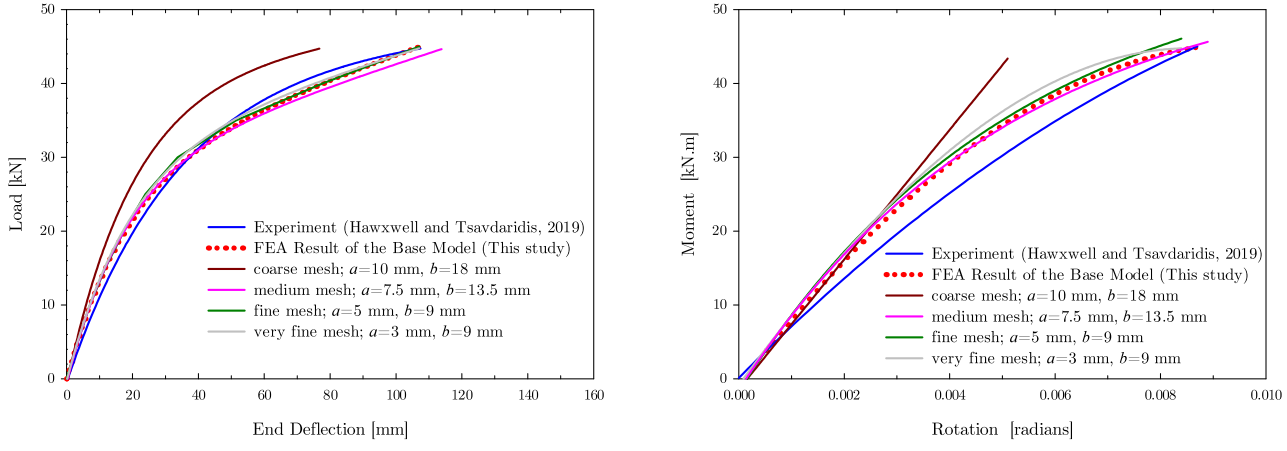

Fig. 11. The comparison of the element sizes used in mesh convergence study.

reliable FE model. A visual comparison between the experimental and FEA model results is shown in Figs. 14 and 15. Note that the deflection in the vertical direction is around 107 mm for the maximum rotation, corresponding to 43 kN for the base model (see Fig. 14). At this maximum load, the failure mechanisms observed in the experiment and the results obtained from the FEA model are compared in Fig. 15. It is observed that the primary beam experienced excessive rotation and local buckling occurred on the connection side of the primary beam flange.

3.2. Parametric study

The experiments were conducted for the baseline case. The effects of several parameters have been investigated to gain comprehensive

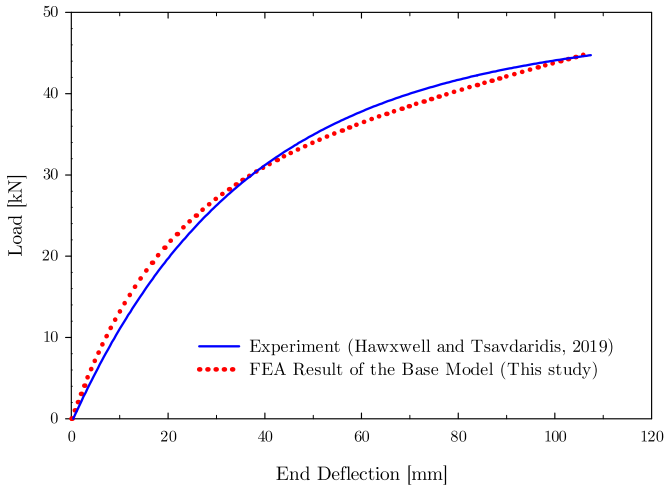

Fig. 12. The comparison of Hawxwell and Tsavdaridis' study [23] and FE base model results through load vs. end deflection (t_1 = 10 mm, t_2 = 10 mm, L_{sb} = 1 m, S_{sb} = 406 × 140 × 39UB, h = −100 mm).

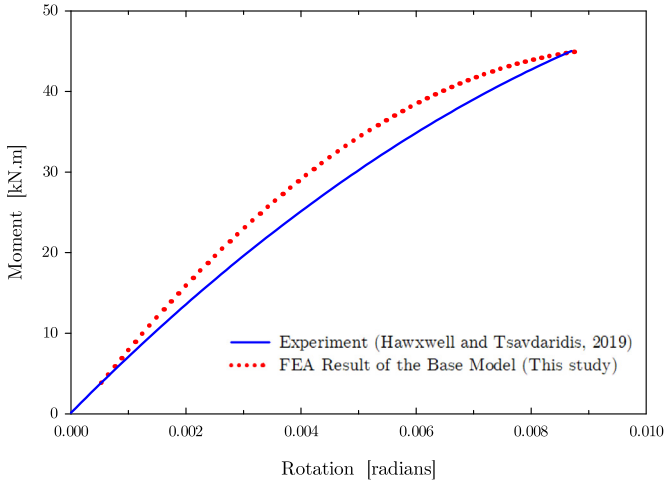

Fig. 13. The comparison of Hawxwell and Tsavdaridis' study [23] and the FE base model results through moment vs. rotation (t_1 = 10 mm, t_2 = 10 mm, L_{sb} = 1 m, S_{sb} = 406 × 140 × 39UB, h = −100 mm).

knowledge about connection behavior. The validated FE model is used as a basis for the parametric study and will be called the base model hereinafter. The design of steel structures tends to involve two stages; the frame design followed by the connection design; therefore, the varying parameters are split into two categories.

1. Parameters controlled by the frame design:
   - span length of the secondary beam; 1 m < L_{sb} < 12 m
   - secondary beam section size; S_{sb} = 406 × 140 × 39UB (Base Model), 406 × 140 × 46UB, 406 × 140 × 53UB, 406 × 178 × 54UB, 406 × 178 × 60UB, 406 × 178 × 67UB, 406 × 178 × 74UB, 406 × 178 × 85UB
   - level difference between primary beam and secondary beam; $h = -200, -100, 0, 100, 200$ mm
2. Parameters controlled by the connection design:
   - stiffener plate thickness; $t_1 = 6, 8, 10, 12, 15, 20$ mm
   - end plate thickness; $t_2 = 6, 8, 10, 12, 15, 20$ mm
   - primary end plate type FDPEP, PDPEP
   - the number of bolt rows

Table 2
Mesh size parameters used in the mesh convergence study.

Mesh Type	a [mm]	b [mm]
coarse mesh	10	18
medium mesh	7.5	13.5
fine mesh	5	9
very fine mesh	3	9

Table 3
Rotation amount at 40 kN load for various mesh types in [radians].

Experiment [23]	Mesh Type	Error [radians]	% Error
7.2e−3	coarse mesh	4.7e−3	34.7
	medium mesh	6.7e−3	7
	fine mesh	6.2e−3	13.9
	very fine mesh	6.2e3	13.9

Table 4
End deflection at 40 kN load for various mesh types in [mm].

Experiment [23]	Mesh Type	Error [mm]	% Error
74	coarse mesh	51.7	30
	medium mesh	85.5	15.5
	fine mesh	77.7	5
	very fine mesh	77.8	5

Table 5
Parametric Study Table.

Parameters
Effect of stiffener thickness (t_1) in [mm]
6/8/10/12/15/20
Effect of end plate thickness (t_2) in [mm]
6/8/10/12/15/20
Effect of the secondary beam span length (L_{sb})
1 m to 12 m in 1 m increments
Effect of the secondary beam section size (S_{sb}) in [mm]
406 × 140 × 39UB
406 × 178 × 54UB
406 × 178 × 60UB
406 × 178 × 67UB
406 × 178 × 74UB
406 × 178 × 85UB
Effect of primary beam section size (S_{pb}) in [mm]
406 × 140 × 39UB
406 × 140 × 53UB
406 × 178 × 54UB
406 × 178 × 85UB
Effect of difference in level of beams h in [mm]
−200/−100/0/+100/+200
Effect of end plate type
FDPEP
PDPEP
Effect of bolt rows
Row 2 removed
Row 3 removed
No bolts removed

The connection's behavior on various beam layouts and geometries – often determined by the frame design – is identified in the first category. In contrast, the second category investigates the impact of altering the connections and its components' design. A list of parameters and the corresponding values that are the subject of this study are given in Table 5.

In the following discussion, the effect of several parameters, including the thickness of the stiffener and end plates, the span length and the section size of the secondary beam, the level difference of beams, partial depth primary end plate, and the number of bolt rows on the moment–rotation response will all be specifically examined in detail. Moreover, the failure zones and mechanism responsible for the failure in the beam-to-beam connections are described. Note that the load is

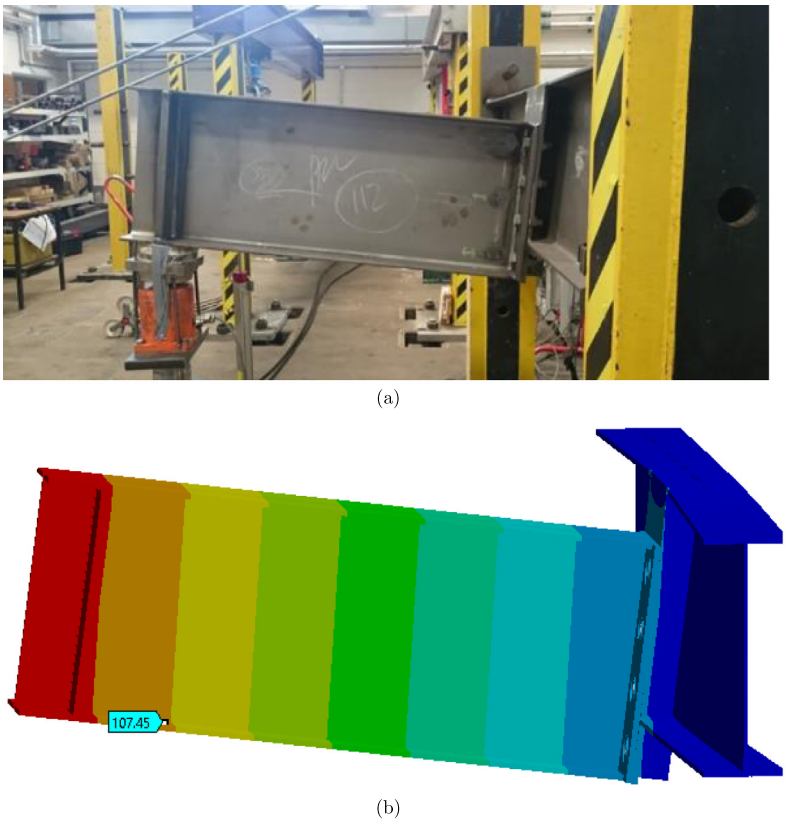

Fig. 14. The comparison between the experimental setup and the FEA model regarding the maximum rotation captured: (a) experimental setup [23] (b) FEA model.

increased for each scenario until the strength capacity of the connection determined by the ultimate strength of the S355 steel is reached. For each case, the moment corresponding to this failure load is presented in the related table.

3.2.1. Effect of the thickness of the stiffeners, t_1

As shown in Fig. 16, all the analyses had the same thing: three prominent failure areas. Zone 1, shown in Fig. 16a, represents the lower side of the lower stiffener. Zone 2, shown in Fig. 16b, is the upper side of the secondary end plate encompassing the four upper bolts. Zone 3, shown in Fig. 16b, is the region on the primary end plate where the secondary end plate applies pressure. In Fig. 17, the equivalent stress distribution patterns near the primary to the secondary beam connection are shown for various thicknesses of the upper and the lower stiffeners labeled as t_1 (See Fig. 3). The results for thicknesses between 6 and 12 mm demonstrated that Zone 1 begins to yield first when linearly increasing force reaches greater values.

On the other hand, for stiffeners thicker than 12 mm, Zone 3 becomes the failure region, where the primary end plate is subject to pressure from the secondary end plate. Note that when connection stiffeners become thicker, the height/thickness ratio (slenderness) decreases, preventing local buckling effects on the stiffener. Thus, the failure region shifts toward the end plates.

The moment–rotation results are shown in Fig. 18, and the failure zones depending on the thickness variation, are listed in Table 6. For each scenario, the simulation is ended whenever a connection component reaches the ultimate tensile strength. It is clearly seen that for a fixed rotation, the moment capacity of the secondary beam is higher for thicker stiffeners. For a fixed moment, thinner stiffeners allow more rotation than thicker stiffeners (see Fig. 18).

3.2.2. Effect of the thickness of the end plates, t_2

In Fig. 19, the equivalent stress distribution patterns of the connection components are shown as the end plate thickness varies from 6 mm to 20 mm. 6 mm thickness is considered for thin-walled steel members, yet it has been included for comparison. The connection with the thinnest end plate is the most flexible one and causes a failure mechanism on the secondary end plate and around the two bolts at the top row named Zone 2. On the other hand, there are no stresses which would cause failure in Zone 1 and Zone 3. For t_2 = 8 mm, the equivalent stress distribution at the loading is given in Fig. 19b. In this case, yielding occurs in all three zones. For t_2=10 mm, t_2=12 mm, and t_2 = 15 mm, at the loading that causes failures, the stress amount in Zone 2 decreases, and failure zones are determined as Zone 1 and Zone 3. The thickest end plate performs completely different characteristics where failure occurs only in Zone 3, as shown in Fig. 19f. Note that the failure regions and the failure moments for the end plates are listed in Table 7. It can be clearly seen that as the components' slenderness increases (thickness decreases), the ineffective compressive zones expand, thus the moment capacity decreases. Furthermore, the stresses on the secondary end plate steadily reduce despite increasing the loading capacity of the connection from Fig. 20a to 20f. The effect of end plates' thickness variation is given as a multi-line chart in Fig. 21.

Table 6
Stiffener thickness t_1 vs. failure zones.

t_1 (mm)	Figure	Failure Zone	Failure Moment [kN m]
6	Fig. 17a	Zone 1	65
8	Fig. 17b	Zone 1	76
10	Fig. 17c	Zone 1, Zone 3	85
12	Fig. 17d	Zone 1, Zone 2, Zone 3	100
15	Fig. 17e	Zone 2, Zone 3	115
20	Fig. 17f	Zone 2, Zone 3	140

3.2.3. Effect of the secondary beam span length, L_{sb}

The span length of the secondary beam, L_{sb}, is an important parameter that affects the initial stiffness boundary of the joint and

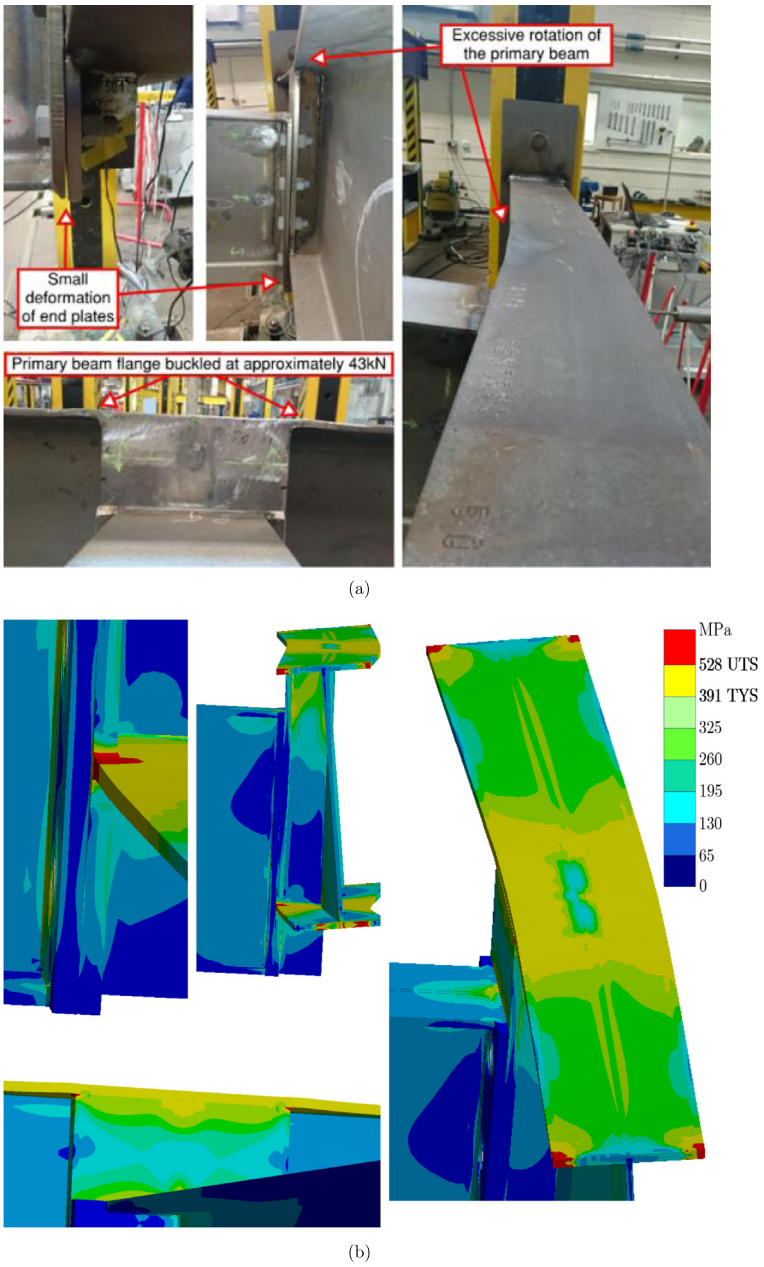

Fig. 15. The comparison between the experimental setup and the FEA model regarding the failure mechanisms captured at 43 kN: (a) experimental setup [23] (b) FEA model.

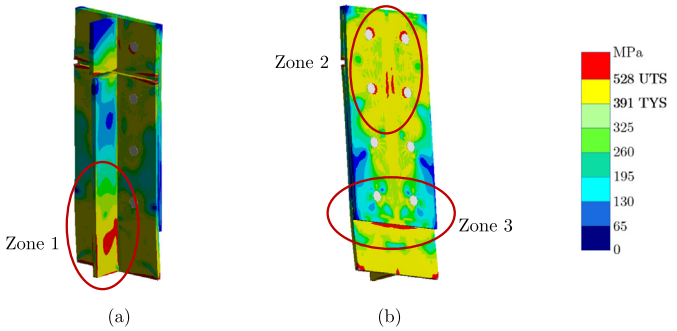

Fig. 16. Failure mechanism zones; the equivalent stress distribution patterns near the primary beam to the secondary beam connection: (a) back view, (b) front view; (M = 80 kN.m, t_1 = 10 mm, t_2 = 8 mm, L_{sb} = 1 m, S_{sb} = 406 × 140 × 39UB, h = −100 mm).

Table 7
End plate thickness t_2 vs. failure zones.

t_2 (mm)	Figure	Failure Zone	Failure Moment [kN.m]
6	Fig. 19a	Zone 2	55
8	Fig. 19b	Zone 1, Zone 2, Zone 3	80
10	Fig. 19c	Zone 1, Zone 3	85
12	Fig. 19d	Zone 1, Zone 3	102
15	Fig. 19e	Zone 1, Zone 3	110
20	Fig. 19f	Zone 3	140

determines the transition from nominally pinned classification to semi-rigid classification. The beams' initial stiffness boundaries ($S_{j.ini}$) are calculated for the range from L_{sb} = 1 m to 12 m, which is commonly used in steel structure applications. $S_{j.ini}$ is calculated from the standard (BS EN 1993-1) [1] as:

$$S_{j.ini} = \frac{EI_b}{2L_{sb}}, \tag{4}$$

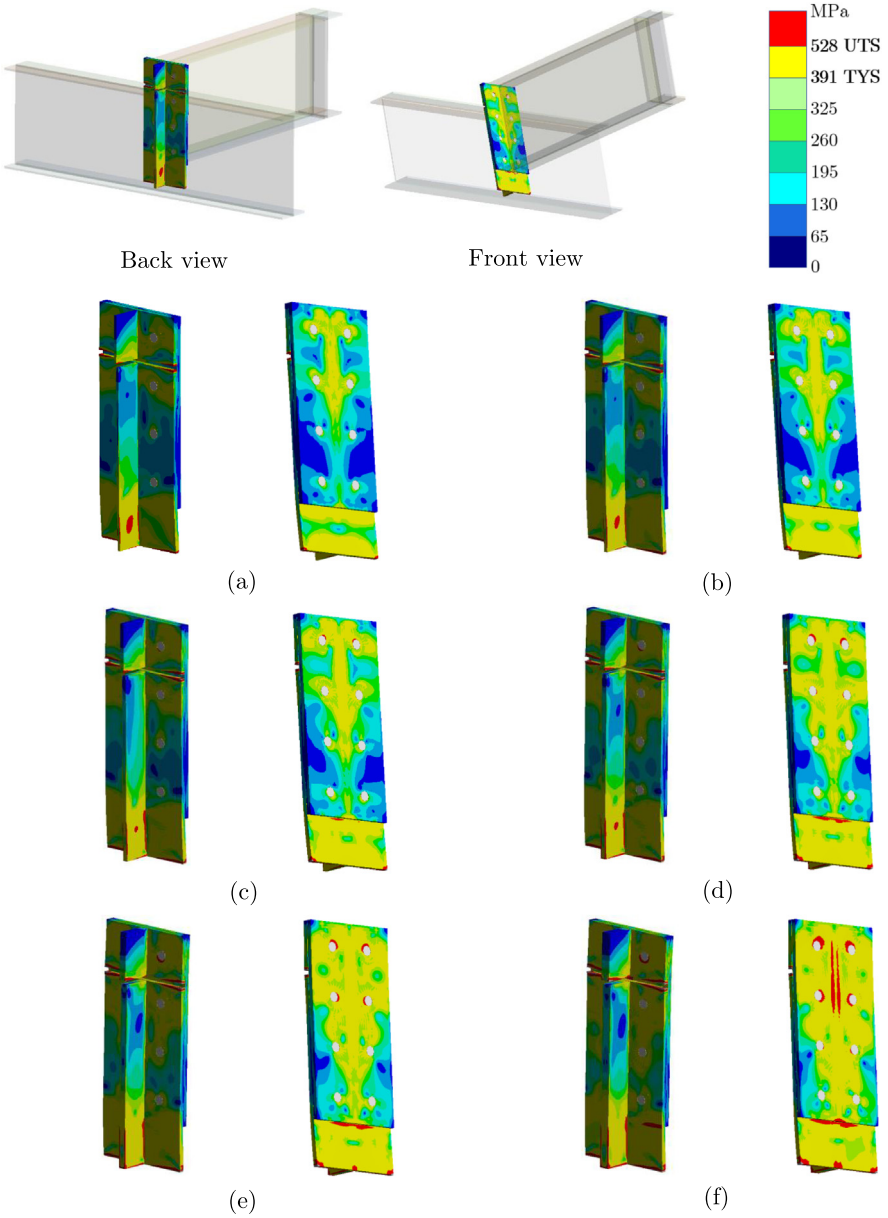

Fig. 17. Back view, the effect of the stiffener thickness t_1, the equivalent stress distribution patterns near the primary beam to secondary beam connection: (a) $t_1 = 6$ mm, (b) $t_1 = 8$ mm, (c) $t_1 = 10$ mm, (d) $t_1 = 12$ mm, (e) $t_1 = 15$ mm, (f) $t_1 = 20$ mm ($t_2 = 10$ mm, $L_{sb} = 1$ m, $S_{sb} = 406 \times 140 \times 39$UB, $h = -100$ mm).

where I_b is the secondary beam's second moment of area (0.000125 m^4), and E is the elastic modulus (210 GPa).

The strength of the joints can generally be classified according to initial stiffness or moment capacity. Generally, there are three types of beam connections, namely nominally pinned (flexible, simple), semi-rigid (partially rigid), and rigid (fully rigid). According to the initial stiffness gradients of different span lengths, the classifications are listed in Table 8, and the initial slopes in moment–rotation curves are given in Fig. 22. It is interpreted from Fig. 22 that as the secondary beams get shorter (or L_{sb} decreased), the slope, $S_{j.ini}$ increases. Thus the probability of the connections being classified as nominally pinned becomes higher.

3.2.4. Effect of the secondary beam section size, S_{sb}

Although section size variation in the secondary beam does not significantly affect the connection's behavior, it changes the classification boundary based on moment strength. According to BS EN 1993-1 [1], a joint may be classified as nominally pinned if its design moment resistance M_{Rd} is not greater than 0.25 times the design moment resistance required for a full-strength joint. The section sizes and their related moment capacities are taken from the Tata Steel interactive blue book [25], and corresponding moment capacity values are given in Table 9. The strength classification is made by evaluating Table 9 and Fig. 23 together. The results show that the boundary level, based on moment strength, is higher relatively for larger section sizes, as shown in Fig. 23, meaning that stronger connections can be used for larger beams and that smaller beams require more ductile connections to be classified as nominally pinned.

3.2.5. Effect of the beam level difference, h

In steel structures, there can be a level difference between the beams due to architectural concerns. Five different beam level differences (−200 mm, −100 mm, 0 mm, +100 mm, and +200 mm) are considered to observe the effect of this variation. A negative value of h means that the secondary beam is translated from the primary beam in the $-z$ direction as in Fig. 5. Fig. 24 shows the results of the moment–rotation relationship related to the level difference between the primary beam and secondary beam. It is seen that the stiffest behavior is observed in

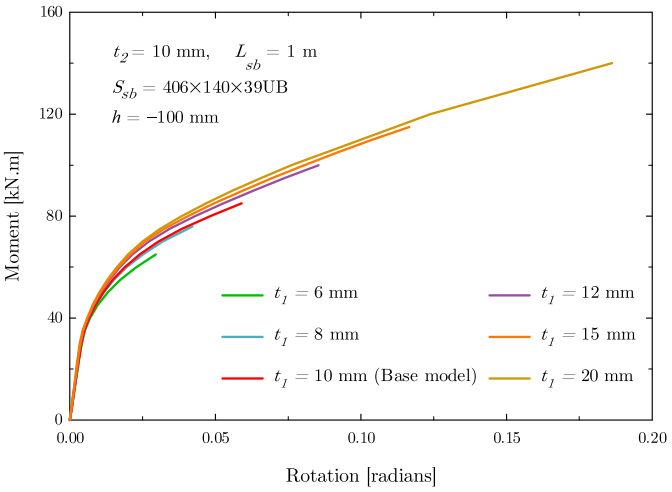

Fig. 18. The effect of upper and lower stiffener thickness t_1 on the moment–rotation behavior of the secondary beam.

Table 8
Initial stiffness gradient calculations for various spans (L_{sb})

Span [m]	S_j	Moment	Strength classification
	[kN m/rad×10^3]	[radians×10^{-3}]	in terms of Initial Stiffness
1	13.1	4.9	Nominally Pinned
2	6.5	9.8	Semi-Rigid
3	4.3	14.7	Semi-Rigid
4	3.3	19.6	Semi-Rigid
5	2.6	24.5	Semi-Rigid
6	2.2	29.4	Semi-Rigid
7	1.8	34.3	Semi-Rigid
8	1.6	39.2	Semi-Rigid
9	1.5	44.1	Semi-Rigid
10	1.3	49.0	Semi-Rigid
11	1.2	53.8	Semi-Rigid
12	1.1	58.7	Semi-Rigid

the case where $h = 0$ mm. As the level difference between the secondary and primary end plates increases ($|h| > 0$), both the initial slope and the moment capacity decrease. For a fixed moment, it is also observed that the joint rotates more as the level difference increases. When the cases of $h = 100$ mm and $h = -100$ mm are compared, it is clear that the upper stiffener is located on the tension side for the $h = -100$ mm case and on the compression side for the $h = 100$ mm case, based on the loading. Therefore, the rotation decreases for the $h = -100$ mm case compared to the $h = 100$ mm case since resistance to rotation is increased in the tension zone of the joint. As the rotation values increase, the connection approaches the nominally pinned classification. Equivalent stress distributions of the connection members for the difference in the level of beams are given in Fig. 25. The failure moment values for various beam level differences are listed in Table 10.

Note that the first bolt row positioning in any end-plate connection (extended or flush) is very critical for the connection's moment capacity. The bigger the lever arm produced from the first bolt row to the compressive (lower) flange, the greater the moment capacity obtained. Having the secondary beam in a lower position means that the first bolt row moves toward the compressive flange of the main beam. Thus, the lever arm is smaller than the $h = 0$ connection, leading to a lower level of moment capacity. This is the dominant reason that the overall behavior is altered due to different level positioning.

3.2.6. Effect of the type of primary end plate

The original design is an FDPEP design, which requires a primary end plate welded across the primary beam's depth. An alternative connection design proposed in this study is to provide a PDPEP in which it is not welded to the bottom flange of the primary beam but instead flushes with the bottom of the secondary end plate (see the sketch in Fig. 26). In Figs. 26 and 27, the moment rotation behavior and the equivalent stress distributions of the base model and PDEP model are compared, respectively. It is found that the PDPEP model is less stiff than the FDPEP model, which causes further rotation and reaches the ultimate strength earlier than the FDPEP. It applies pressure to the lower stiffener contact surface, eventually leading to failure. Regarding the initial stiffness, the PDPEP model provides less slope, which makes the connection be classified as nominally pinned. Moreover, PDPEP has a lower moment capacity compared to FDPEP, which makes the joint categorized as nominally pinned.

3.2.7. Effect of the number of bolt rows

The initial design includes four rows of bolts. This section reduces the number of bolts to study the effect on joint characteristics. Since the top (Row 1) and bottom (Row 4) rows must exist as a minimum requirement, the second (Row 2) and the third (Row 3) rows of bolts are removed for the investigation. The removal of bolt row 2 resulted in a minor drop in the initial stiffness, as seen in Fig. 28. Since the connection is subject to a moment causing compression in the flange and tension in the bolts, removing bolt row 2 will have more effect than bolt row 3, as seen in these results. However, removing the second and third bolt rows minimally affects the joint's initial stiffness and moment strength.

3.2.8. Bolt analysis

The axial forces of the bolts with the most severe conditions among all parametric analyzes are given in Table 11. These values are compared with the proof load of the grade 8.8 M20 bolts, which is a threshold value to maintain the bolt's original size and shape. The proof load of the grade 8.8 M20 bolt is 147 kN [26]. Table 11 clearly shows that axial force in any bolt does not exceed the proof load of grade 8.8 M20 bolts. Similarly, the maximum shear forces observed in the bolts are given in Table 12. It is clearly seen in Table 12 that the maximum shear force observed in any bolt in all parametric analyses is 68 kN (Bolt 1 and 8 corresponding to $h = -100$ mm). The shear capacity of grade 8.8 M20 bolt with S355 steel is 91.9 kN. Hence, it can be concluded that the shear force in any bolt does not exceed the shear capacity of the bolt before other components fail.

4. Concluding remarks

One of the requirements for the accurate assessment and construction of steel structures is a good understanding of the moment–rotation behavior of their connections and the correct classification of the joints. Joint classification can vary and is highly dependent on the size and geometry of the beams and connection parts. Three different combinations, namely, FP, PDEP, and EEP connections, were investigated in this paper. Joint classification can vary and is highly dependent on the size and geometry of the beams and connection parts. This parametric study presents the limits of beam-to-beam connections that can be classified as nominally pinned for several key geometric factors.

- When connection stiffeners become thicker, the failure region shifts toward the end plates.
- When the thickness of the upper and lower stiffener (t_1) or end plate thickness (t_2) is doubled from the baseline value (t_1 = 10 mm, t_2 = 10 mm), the failure moment increases by 64.7%.
- When the thickness of the upper and lower stiffener (t_1) or end plate thickness (t_2) is decreased by 40% from the baseline value (t_1 = 10 mm, t_2 = 10 mm), the failure moment decreases by 23.5%.
- The failure moment is reduced by 55% for the beam level difference of $h = 200$ mm as compared to the case where the beams are leveled (i.e., $h = 0$ mm). However, the failure moment is reduced by 45% for the $h = -200$ mm case.

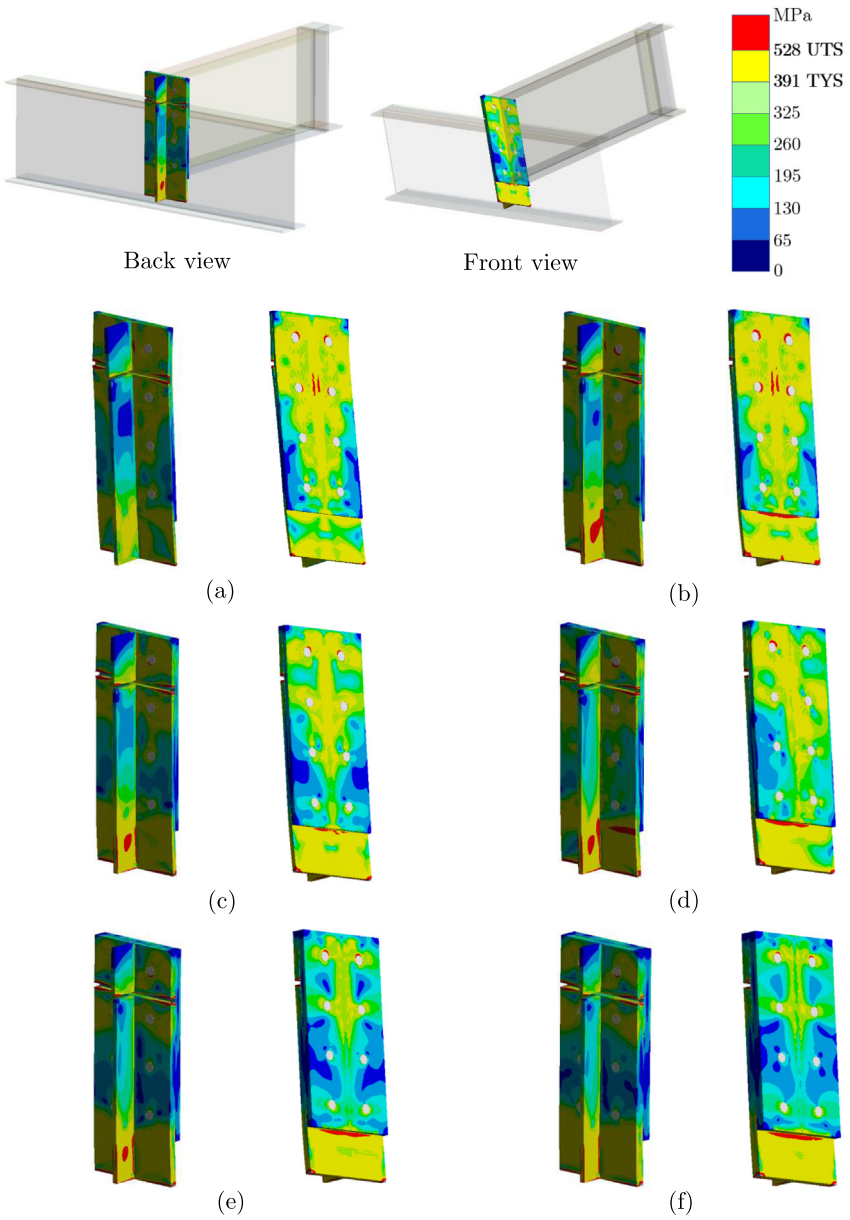

Fig. 19. The effect of the end plate thickness t_2, the equivalent stress distribution patterns near the primary beam to secondary beam connection: (a) $t_2 = 6$ mm, (b) $t_2 = 8$ mm, (c) $t_2 = 10$ mm, (d) $t_2 = 12$ mm, (e) $t_2 = 15$ mm, (f) $t_2 = 20$ mm, ($t_1 = 10$ mm, $L_{sb} = 1$ m, $S_{sb} = 406 \times 140 \times 39$UB, $h = -100$ mm).

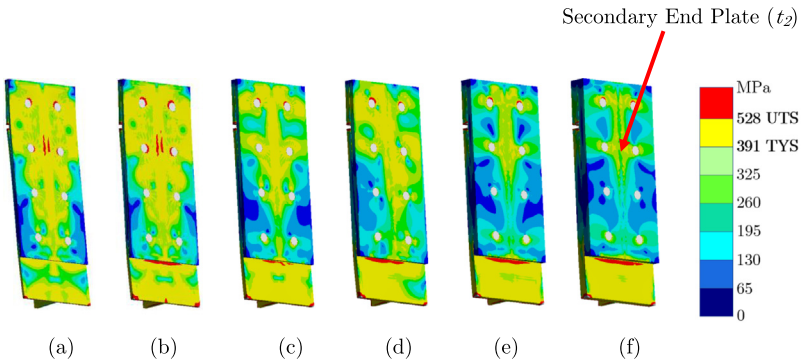

Fig. 20. The equivalent stress distribution patterns near the primary beam to the secondary beam connection for t_2: (a) $t_2 = 6$ mm, (b) $t_2 = 8$ mm, (c) $t_2 = 10$ mm, (d) $t_2 = 12$ mm, (e) $t_2 = 15$ mm, (f) $t_2 = 20$ mm, ($t_1 = 10$ mm, $L_{sb} = 1$ m, $S_{sb} = 406 \times 140 \times 39$UB, $h = -100$ mm).

Table 9
Secondary beam section sizes vs moment resistance values.

Section Size	M_{Rd} (kN m)	0.25 $\times M_{Rd}$ (kN m)	Strength Classification in terms of Moment Capacity
406 × 140 × 39UB	257	64.25	Semi-Rigid
406 × 140 × 46UB	315	78.75	Semi-Rigid
406 × 140 × 53UB	366	91.50	Nominally Pinned
406 × 178 × 54UB	373	93.25	Nominally Pinned
406 × 178 × 60UB	426	106.50	Nominally Pinned
406 × 178 × 67UB	479	119.75	Nominally Pinned
406 × 178 × 74UB	533	133.25	Nominally Pinned
406 × 178 × 85UB	597	149.25	Nominally Pinned

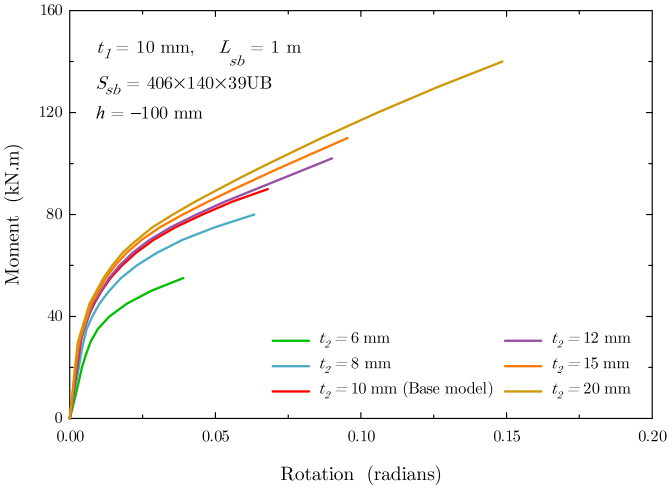

Fig. 21. The effect of the end plate thickness t_2 on the moment–rotation behavior of the secondary beam.

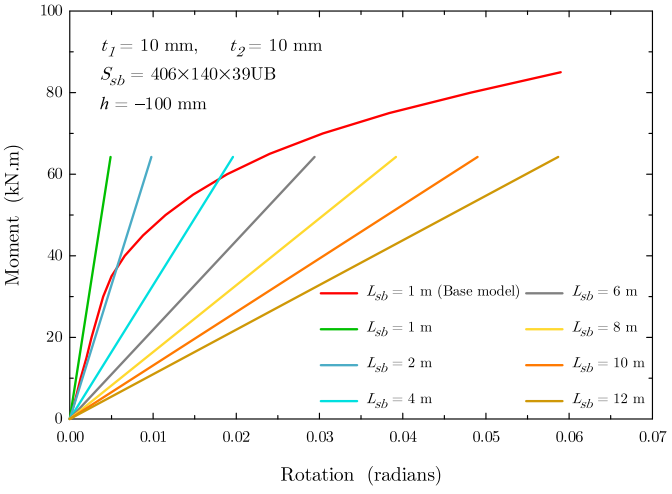

Fig. 22. The effect of the secondary beam span length L_{sb} on the moment–rotation behavior of the secondary beam.

Table 10
Beam Level Difference h vs. failure moments.

h (mm)	Figure	Failure Moment [kN.m]
200	Fig. 25a, b	45
100	Fig. 25c, d	80
0	Fig. 25e, f	100
−100	Fig. 25g, h	85
−200	Fig. 25i, j	55

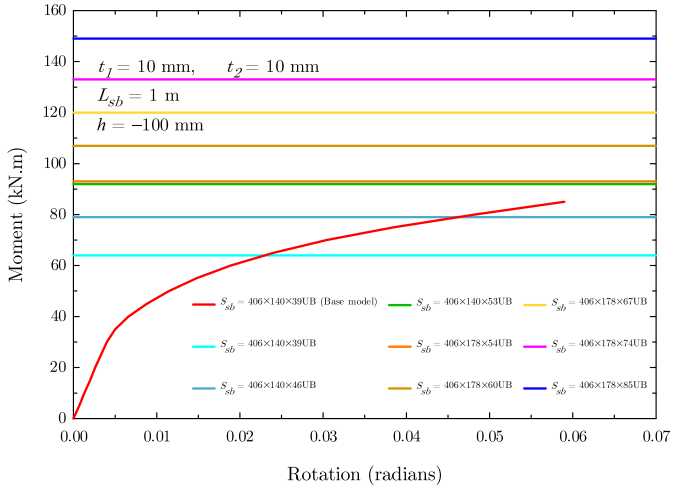

Fig. 23. The effect of the secondary beam section size S_{sb} on the moment–rotation behavior of the secondary beam.

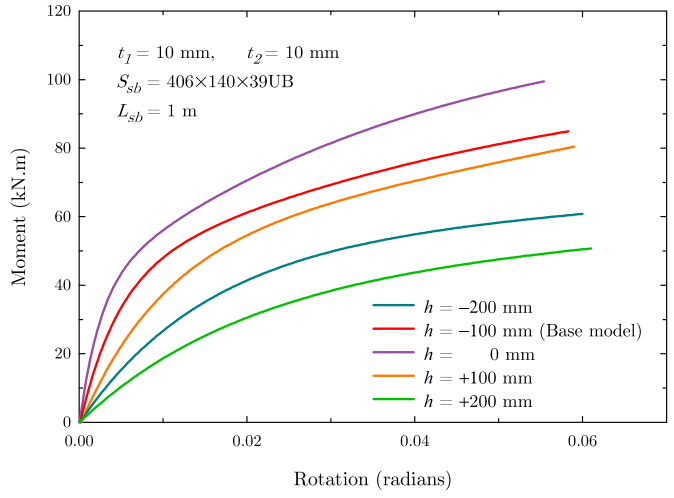

Fig. 24. The effect of the difference in the beams' level h on the moment–rotation behavior of the secondary beam.

- The results show that the larger the section size, the higher the boundary at which the joint changes from the nominally pinned category to the semi-rigid category. Therefore, connections with larger cross-section sizes can still be interpreted as being nominally pinned, even if more rigid connections were used. Connections with smaller section sizes, on the other hand, should bear connection applications with a higher level of ductility so they can be classified as nominally pinned.

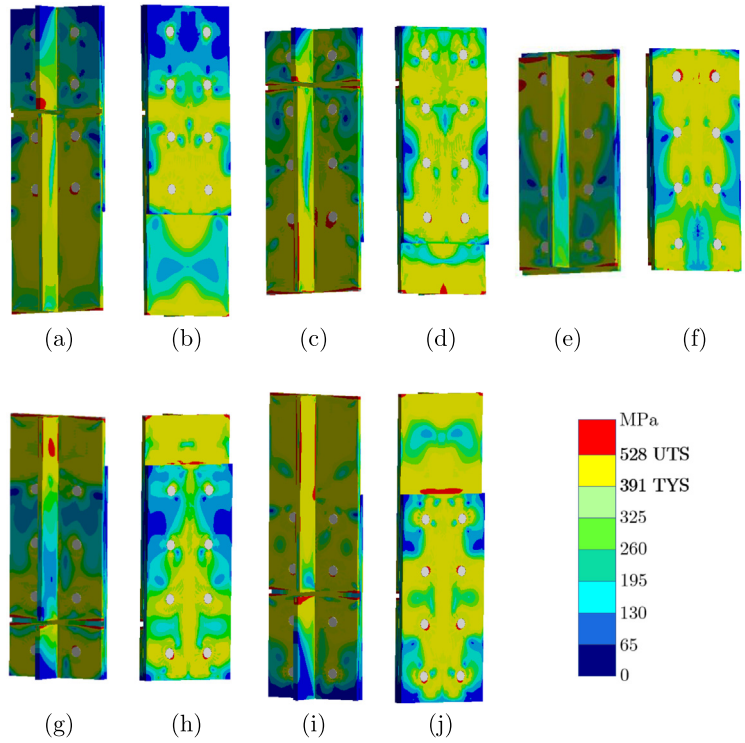

Fig. 25. The equivalent stress distribution patterns near the primary beam to the secondary beam connection for various values of h: (a) $h = +200$ mm, back view, (b) $h = +200$ mm, front view, (c) $h = +100$ mm, back view, (d) $h = +100$ mm, front view, (e) $h = 0$ mm, back view, (f) $h = 0$ mm, front view, (g) $h = -100$ mm, back view, (h) $h = -100$ mm, front view, (i) $h = -200$ mm, back view, (j) $h = -200$ mm, front view; ($t_1 = 10$ mm, $t_2 = 10$ mm, $L_{sb} = 1$ m, $S_{sb} = 406 \times 140 \times 39$UB).

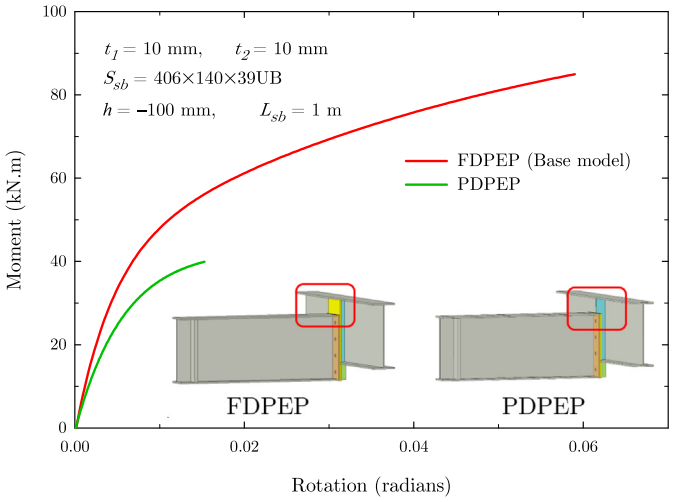

Fig. 26. The comparison of FDPEP vs. PDPEP primary end plate on the moment–rotation behavior of the secondary beam.

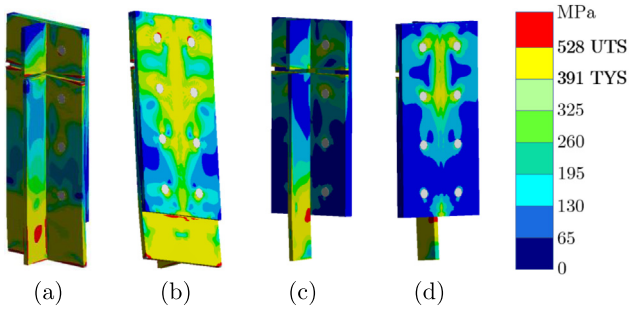

Fig. 27. The equivalent stress distribution patterns near the primary beam to the secondary beam connection for FDPEP and PDPEP: (a) FDPEP, back view, (b) FDPEP, front view (c) PDPEP, back view (d) PDPEP model, front view; ($t_1 = 10$ mm, $t_2 = 10$ mm, $L_{sb} = 1$ m, $S_{sb} = 406 \times 140 \times 39$UB), $h = +100$ mm.

Table 11
Maximum bolt axial forces observed in the parametric study corresponding to $t_2 = 20$ mm.

Bolt No	Axial Force [kN]
1	122
2	139
3	27
4	80
5	80
6	31
7	141
8	119

Table 12
Maximum bolt shear forces observed in the parametric study corresponding to $h = -100$ mm.

Bolt No	Shear Force at I [kN]	Shear Force at J [kN]
1	68	68
2	63	63
3	35	35
4	16	15
5	16	15
6	35	35
7	63	63
8	68	68

- As the level difference (h) between the primary end plate and secondary end plate increases, the initial stiffness and strength of the connection decrease.

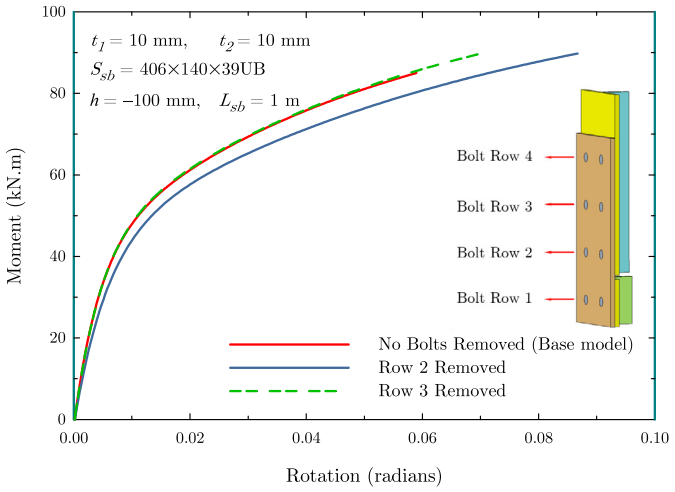

Fig. 28. The effect of the number of bolt rows on the moment–rotation behavior of the secondary beam.

- Removing one row of bolts between the top and the bottom rows (second or third row) has minimal effects on both the initial stiffness and the strength capacity of the connection.

Finally, cyclic loading protocol application with the use of common or prestressed bolts could be a future topic to study.

CRediT authorship contribution statement

Samet Eltaş: Visualization, Validation, Investigation, Formal analysis, Data curation. **Mehmet Ali Güler:** Writing – review & editing, Software, Resources, Project administration, Methodology, Funding acquisition. **Konstantinos Daniel Tsavdaridis:** Writing – review & editing, Writing – original draft, Validation, Supervision, Project administration, Conceptualization. **Christos E. Sofias:** Writing – review & editing, , Writing – original draft, Validation, Methodology. **Bora Yıldırım:** Writing – original draft, Validation, Formal analysis, Data curation.

Declaration of competing interest

The authors declare the following financial interests/personal relationships which may be considered as potential competing interests: On behalf of the co-authorial team. Prof KD Tsavdaridis

Data availability

No data was used for the research described in the article.

References

[1] British Standard, Eurocode 3—Design of steel structures—, BS EN 1993-1 1 (2006) 2005.
[2] M.A. Hadianfard, R. Razani, Effects of semi-rigid behavior of connections in the reliability of steel frames, Struct. Saf. 25 (2) (2003) 123–138.
[3] L.M.C. Simoes, Optimization of frames with semi-rigid connections, Comput. Struct. 60 (4) (1996) 531–539.
[4] Merve Sağıroğlu, Mahyar Maali, Mahmut Kılıç, Abdulkadir Cüneyt Aydın, A novel approach for bolted T-stub connections, Int. J. Steel Struct. 18 (3) (2018) 891–909.
[5] Rohola Rahnavard, Navid Siahpolo, Mohammad Naghavi, Akbar Hassanipour, Analytical study of common rigid steel connections under the effect of heat, Adv. Civ. Eng. 2014 (2014).
[6] W.G. Altman, A. Azizinamini, J.H. Bradburn, J.B. Radziminski, Moment-Rotation Characteristics of Semi-Rigid Steel Beam-Column Connections, National Technical Information Service, 1983.
[7] David Anderson, Zoubir Benterkia, Analysis of semi-rigid steel frames and criteria for their design, J. Construct. Steel Res. 18 (3) (1991) 227–237.
[8] Miklos Ivanyi, Semi-Rigid Joints Instructural Steelwork, Springer, 2000.
[9] A Bahaz, S Amara, Jean-Pierre Jaspart, Jean-François Demonceau, Analysis of the behaviour of semi rigid steel end plate connections, in: MATEC Web of Conferences, Vol. 149, EDP Sciences, 2018, p. 02058.
[10] Vitor Rodrigues Gomes, André Tenchini, Luciano Lima, Pedro Vellasco, Robustness assessment of semi-rigid steel multi-storey frames, in: Structures, Vol. 25, Elsevier, 2020, pp. 849–860.
[11] Rasha K Al-Fisalawi, AL-Hadithy Laith Khalid, Mustafa Kamal Al-Kamal, Performance of semi-rigid steel connections under monotonic and cyclic loadings: a review, 2021.
[12] F. Iannone, M. Latour, V. Piluso, G. Rizzano, Experimental analysis of bolted steel beam-to-column connections: Component identification, J. Earthq. Eng. 15 (2) (2011) 214–244.
[13] F. Barbagallo, M. Bosco, E.M. Marino, P.P. Rossi, Seismic design and performance of dual structures with BRBs and semi-rigid connections, J. Construct. Steel Res. 158 (2019) 306–316.
[14] Hao Wang, Bo Yang, Xu-Hong Zhou, Shao-Bo Kang, Numerical analyses on steel beams with fin-plate connections subjected to impact loads, J. Construct. Steel Res. 124 (2016) 101–112.
[15] Ying Zhang, Shan Gao, Lanhui Guo, Jiayi Qu, Sheliang Wang, Ultimate tensile behavior of bolted T-stub connections with preload, J. Build. Eng. 47 (2022) 103833.
[16] Mohammad Jobaer Hasan, Mahmud Ashraf, Safat Al-Deen, Sukanta Kumer Shill, Brian Uy, Stainless steel top-seat angle beam-to-column connection: Full-scale test and analytical modelling, in: Structures Vol. 34, Elsevier, 2021, pp. 4322–4338.
[17] Xuesen Chen, Gang Shi, Experimental study on seismic behaviour of cover-plate joints in high strength steel frames, Eng. Struct. 191 (2019) 292–310.
[18] Yasin Onuralp Özkılıç, Cem Topkaya, Extended end-plate connections for replaceable shear links, Eng. Struct. 240 (2021) 112385.
[19] Manuel Lopez, Alfonso Loureiro, Ruth Gutierrez, Jose M. Reinosa, A new analytical formulation for the stiffness and resistance of the additional plate in bending in beam-to-beam steel joints, Eng. Struct. 228 (2021) 111476.
[20] Kestutis Urbonas, Alfonsas Daniūnas, Behaviour of semi-rigid steel beam-to-beam joints under bending and axial forces, J. Construct. Steel Res. 62 (12) (2006) 1244–1249.
[21] Vijayakumar Natesan, Mahendrakumar Madhavan, Performance of CFS beam-to-beam bolted connection using clip angle and flange strip: Experimental investigation, J. Struct. Eng. 145 (10) (2019) 04019101.
[22] M.R. Mohamadi-Shooreh, M. Mofid, S.L. McCabe, Empirical model of the moment-rotation curve of beam-to-beam bolted flush endplate connections, J. Struct. Eng. 139 (1) (2013) 66–72.
[23] Daniel Allan Hawxwell, Konstantinos Daniel Tsavdaridis, Beam-to-beam eccentric end plate connections-Experimental comparison to fin plate and partial-depth end plate connections, Structures 19 (2019) 411–423.
[24] Jinming Zeng, Wei Lu, Juha Paavola, Ultimate strength of a beam-to-column joint in a composite slim floor frame, J. Construct. Steel Res. 140 (2018) 82–91.
[25] Tata Steel Europe Ltd., Tata Steel Section Interactive Blue Book, 2015.
[26] EDGE ENGINEERS, LLC., BS EN ISO 898-1: Minimum ultimate tensile loads and proofing loads.